Study on Impact Toughness of C-Mn Multilayer Weld Metal at −60°C

Ferrite located in the crack initiation region greatly influences the propagation

BY J. H. CHEN, T. D. XIA and C. YAN

ABSTRACT. A comparative study has been carried out on the toughness of specimens of the C-Mn multilayer weld steel and that of the specimens simulated with the various reheating cycles by using the weld thermal-restraint stress and strain cycle simulator. It proved that the region initiating the cleavage crack, *i.e.*, the weakest region in the multilayer weld metal impact-fractured at −60°C (−76°F), is just the region having the lowest toughness among various reheated zones. The toughness of weld metal depends upon the toughness value of this weakest region. Heat input and alloying elements, such as manganese, titanium and boron, affected the toughness of weld metal by changing the toughness of the weakest region in the multilayer weldment.

Introduction

There are as-deposited weld metals and weld metals reheated to various temperatures by the subsequent beads in a multilayer weldment (Ref. 1). Generally, improving the microstructures and mechanical properties of the as-deposited weld metals will increase that of the multilayer weldment. Stout, *et al.* (Ref. 1), and Evans (Ref. 2), concluded that the toughness of weld metal was improved by a successive reheating process. The greater the reheated zone, the higher is the toughness of a C-Mn multilayer weldment. However, when the heat input is very high, even though the weld metal contains a large amount of reheated weld metal, toughness decreases greatly. Up to now, there was not a definite relationship between the microstructures and the properties of as-deposited weld metal and that of reheated weld metal.

To improve impact toughness of the C-Mn weld metal, some well-known physical metallurgy principles are used. The most important principle is adding alloying elements, such as manganese, titanium and boron, to the weld metal. Evans (Ref. 3) considered when the Mn content was 1.4 wt-% the toughness of the weld metal was the highest.

Several investigations discovered that the addition of a combination of titanium and boron into the weld metal effectively produces a fine acicular ferrite microstructure that displays a satisfactory low-temperature toughness (Refs. 4–7), especially at the high heat input (Refs. 8, 9) levels. A large volume fraction of acicular ferrite (up to 95%) can be obtained by maintaining boron and titanium contents between 40–45 ppm and 400–500 ppm, respectively. But the question is, with the higher heat input, how do titanium and boron affect the microstructure and toughness of the entire weld metal?

In this paper, an investigation of the microstructure and impact toughness of 12 different welds, with varying manganese, titanium, boron and heat input is described. Impurity elements such as P, S, O and N were strictly controlled. Thermal simulation was used on the weld samples. A more fundamental understanding of the mechanisms controlling the onset of cleavage fracture of the C-Mn steel multilayer weld metal at low temperature and the complex interrelationship between the microstructure and the weakest zone of fractured weld metal are developed.

Kott and coworkers (Refs. 10–12) studied the fracture behavior of C-Mn welds in detail. He concluded that cleavage fracture in welds often originated from cracking of oxide inclusions, in particular those situated in the coarse-grained ferrite, and that the size distribution of these inclusions had a significant effect on the fracture toughness. Two of the present authors (Ref. 13) have investigated the original nucleus of cleavage and the weakest zone in the fractured C-Mn weld metal and found that the toughness of the as-deposited metal could be improved by

KEY WORDS

Impact Toughness
C-Mn Steel Weld
Multilayer Welds
Thermal Simulation
Low-Temp. Toughness
Toughness at −60°C
SMA Welding
Impact Fracture
Fracture Metallography
Simulated Microstructure

J. H. CHEN, T. D. XIA and C. YAN are with the Welding Research Institute, Gansu University of Technology, Lanzhou, Gansu, People's Republic of China.

Table 1 — Chemical Compositions of the Weld Metals[(a)] and Heat Input

Alloy System	No.	E[(b)]	C	Si	Mn	S	P	Ti	B	O	N
C-Mn-Ti with	501	1.0	0.06	0.33	0.68	0.015	0.024	*	*	*	*
increasing	601	1.0	0.05	0.42	1.04	0.013	0.012	0.019	0	*	*
Mn content	602	2.0	0.06	0.41	0.99	0.013	0.013	0.018	0	*	*
	604	4.0	0.06	0.35	1.01	0.012	0.013	0.013	0	*	*
	701	1.0	0.06	0.31	1.34	0.012	0.021	0.030	*	300	190
	801	1.0	0.06	0.33	1.98	0.012	0.019	*	*	*	*
C-1.0Mn-Ti-B	611	1.0	0.04	0.31	1.07	0.017	0.010	0.020	36	*	*
	612	2.0	0.05	0.28	1.07	0.015	0.015	0.018	33	*	*
	614	4.0	0.04	0.27	1.06	0.016	0.012	0.016	29	*	*
C-1.36Mn-Ti	631	1.0	0.05	0.34	1.36	0.013	0.015	0.024	43	300	190
-B	632	2.0	0.06	0.34	1.34	0.012	0.014	0.024	41	*	*
	634	4.0	0.07	0.31	1.26	0.013	0.013	0.019	36	*	*

(a) All concentrations are in wt-%, except for boron, oxygen and nitrogen, which are given in weight ppm.
(b) E indicates nominal heat input in terms of KJ/mm.
* Not measured.

adding appreciable Mn. The weakest zone was the coarsest ferrite grain and could be changed from the deposited metal to the coarse ferrite grain zone in the reheated weld metal. Work is presently being conducted to further clarify the following problems: 1) which zone in the multilayer weldment has the lowest toughness and is the weakest region of the fractured weld metal? 2) whether the toughness of the weakest zone determines that of weld metal in whole?

Experimental Procedure

Materials

Table 1 shows the chemical compositions of the weld metals used in the present study produced by three kinds of covered electrodes, each operated at three heat input levels. The schematics of the sampling of test specimens is shown in Fig. 1. All welding was made in accordance with ISO 2560, with a current of 170 A, a voltage of 23 V and a maximum interpass temperature of 150°C (302°F). The welding speed was changed from 4.0 mm/s to 0.9 mm/s, and the nominal heat inputs were 1.0, 2.0 and 4.0 kJ/mm (25, 51 and 102 kJ/in.), respectively. Welding bead arrangements are shown in Fig. 1.

Thermal Simulation Test

Theoretically, the specimens to be simulated must be as-deposited ones, but the single bead produced by shielded metal arc welding is too small in size to obtain a complete specimen. According to Evans (Ref. 14)[1], when the specimen was reheated above A_{c3}, the microstructure of the simulated metal was independent of whether the specimen was as-deposited or reheated and was only determined by the composition of weld metal and simulating schemes. So it is practicable that instead of the pure as-deposited weld metal, a specimen of multilayer weld metal may be used in simulation studies.

Specimens in the size of 11 X 11 X 55 mm (0.43 X 0.43 X 2.17 in.) were thermally simulated, and standard Charpy V-notch test specimens were made in the size of 10 X 10 X 55 mm (0.39 X 0.39 X 2.17 in.), with 2-mm (0.08-in.) notch depth and 0.25-mm (0.01-in.) root radius.

The thermal cycles of the reheated metal in the multilayer weldments were measured with a tungsten-rhenium thermocouple. The measured parameters for the thermal cycles are shown in Table 2.

Thermal simulation was made with a Thermorestor-W weld thermal-restraint stress-and-strain cycle simulator. Specimens were heated by high-frequency induction and cooled with nitrogen gas. Three specimens were used for each simulating regime shown in Table 2.

Specimen for Initiating Crack in As-Deposited Metal

To determine the weakest region of the weldment, in addition to the multilayer weldment specimen, the specimens shown in Fig. 2 were used. In the impact-fractured specimens shown in Fig. 2, the crack was initiated from the as-deposited metal zone, and its toughness could be measured. These specimens were made by filling up the groove of the specimen shown in Fig. 1 with Nos. 50, 70 and 80 covered electrodes of the C-Mn steel system. The upper beads were then planed out, and a U-type channel was machined in the center of the weldment. This channel was filled up with a single pass with the same covered electrodes of 5.0-mm (0.2-in.) diameter, operated at 230–250 A, which is shown in Fig. 2A. Two kinds of standard impact specimens with different notches were obtained as shown in Fig. 2B

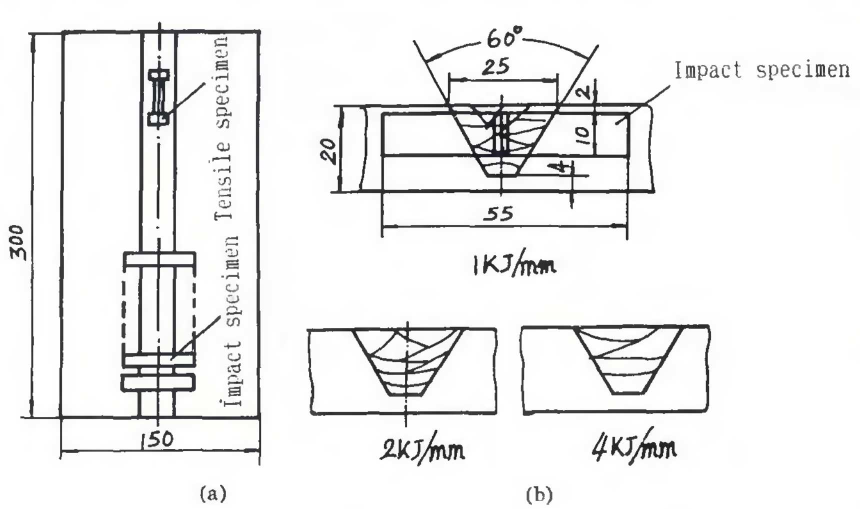

Fig. 1—Schematics of test sample and bead arrangement. A—Test sample; B—bead arrangement.

1. *Evans added, "A memory effect still persists, however, because of slight preferential grain growth in regions adjacent to original fusion boundaries. In addition, prior location of the individual beads is accentuated by the tendency of second phases to be aligned along prior segregation bands."*

Table 2 — Specifications for Simulating Weld Metals(a)

E(kJ/mm)	T_{max} (°C)	t_h(S)	t_H(S)	$t_{T/8}$(S)	$t_{8/5}$(S)	$t_{5/3}$(S)
1.0	1350	10	3	6	12	26
1.0	1150	10	4	3	12	26
1.0	950	9	5	2	12	26
1.0	850	9	6	2	12	26
2.0	1350	27	3	10	32	140
2.0	1150	26	7	7	32	140
2.0	950	25	10	5	32	140
2.0	850	24	13	2	32	140
4.0	1350	77	11	34	65	443
4.0	1150	75	30	22	65	443
4.0	950	73	36	13	65	443
4.0	850	72	49	9	65	443

(a) E is heat input, T_{max} is heating peak temperature, t_h is heating time, t_H holding time at the peak temperature, $t_{T/8}$ the cooling time from T_{max} to 800°C and $T_{8/5}$, $t_{5/3}$ are the cooling times from 800° to 500°C and from 500° to 300°C, respectively.

and Fig. 2C, respectively. The former was called as-deposited metal specimen (AMS) and the latter, mixed weld metal specimen (MMS). The impact tests for both kinds of specimens were carried out at −60°C (−76°F).

Impact and Tensile Test

Impact tests of standard Charpy V-notch specimens were carried out with the instrumented impact machine CIME-30D-CPC at −60°C. Specimens were cooled with ethanol and liquid nitrogen, and the temperature error was controlled within ±2°C (3.6°F) with a temperature sensor. Tensile tests were carried out with the universal tensile test machine SIMAD-ZU-AG-10TA at room temperature.

Fracture Surface and Weakest Region in Impact-Fractured Specimens

The impact-fracture surfaces were observed by scanning electron microscope (SEM). The cleavage crack origins were determined using the secondary electron and the reflected electron image, and tracing back the river pattern line to its origin on the cleavage facet (Ref. 13). The distance L_{tc} between the cleavage origin and the root of the notch was measured. The energy-dispersive x-ray (EDX) was used to identify the kind of the various crack origins by composition. The fracture facet feature surrounding the cleavage origin was observed. After protecting the fracture surface with a transparent film, as shown in Fig. 3A, the metallographic surface perpendicular to the fracture surface was cut, ground and polished just to pass through the crack origin region, and the microstructure of this region was observed by SEM and an optical microscope. The sizes of ferrite grains in this cleavage origin region were measured with a PIAS-1 image processing system. First, a picture of the microstructures in the origin region was taken and the outlines of its constitutes were sketched, then the sizes of the ferrite and the proportion of its constitutes were automatically measured and calculated by the computer image processing system. The remaining cracks parallel to the main crack in the fracture-metallography specimen were examined by SEM in section as shown in Fig. 3B, and the lengths L_{max} of the maximum remaining cracks were measured.

Metallographic Examination of the Simulated Microstructure

The microstructures simulated with various thermal cycles were observed by optical microscope. The microstructures of the simulated specimens having the lowest toughness among all specimens with the same composition were compared with that of the region initiating the multilayer weldment.

Results

Mechanical Tests

The tensile properties of the multilayer weld metal at room temperature are shown in Table 3. The impact toughness of the multilayer weld metal at −60°C are shown in Table 4 and Fig. 4. Figure 5 shows the histogram of the toughness of the specimens simulated with various peak temperatures and tested at −60°C for the various weldments welded with different heat input levels. Figure 6 compared the lowest toughness among all simulated specimens. From these figures, it was revealed that the toughness of weld metals descended as heat input increased, and increased as Mn content increased from 0.8 to 1.5 wt-%. However, when Mn content increased to 1.98 wt-%, the toughness decreased again. With the addition of a small amount of B, the weld metal toughness was improved. At the same heat input level, sample No. 63 weld metal, which contained 1.36 wt-% Mn and the proper amount of Ti and B, had higher toughness at −60°C than the other two kinds of weld metal. It could also be seen that the region that had the lowest toughness was different. For most of the weld metals, the regions that were reheated at the peak temperature of 1350°C (2462°F) or 1350° + 850°C (2462° + 1562°F), except for sample No. 801, which contained 1.98 wt-% Mn, the weakest region was that reheated at 1150°C (2102°F). The toughness of the region having the lowest toughness in the weld metal contained 1.5 wt-% Mn, and the proper amount of Ti and B, and it was obviously higher than that of the weld metal containing lower Mn content.

As shown in Table 4, the toughness of the as-deposited metal was lower than that of the multilayer weld metal, but the former were higher than that of the lowest toughness of the simulated specimens. It proved that the deposited metal probably was not necessarily the region having

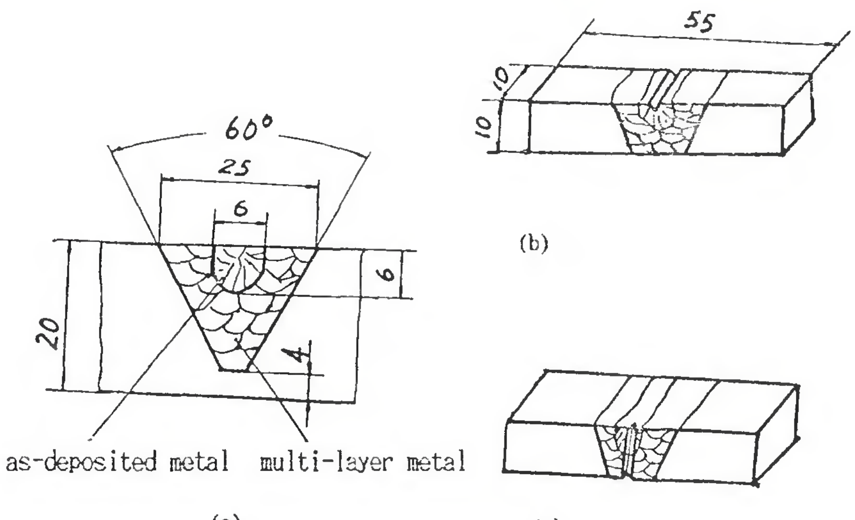

Fig. 2 —Charpy specimens notched in the different weld metals. A —Weld metal; B— notched in the as-deposited metal; C —notched in the mixed weld metal zone.

Table 3 — The Mechanical Properties of Weld Metals at R.T.

No.	σ_s (MN/m^2)	σ_b (MN/m^2)	δ (%)
501	391	490	32.7
701	428	557	29.3
801	448	613	28.7
601	477	590	28.5
602	414	511	32.8
604	392	511	34.4
611	423	539	30.0
612	394	498	34.0
614	358	478	36.3
631	474	567	27.9
632	438	531	29.5
634	382	508	29.7

Table 4 — The Impact Absorbed Energy of the Specimens Tested at −60°C, J

		Peak Temperature Simulated (°C)							
No.	Weld Metal	1350	1150	950	1350 + 850	850	AMS[a]	MMS[b]	850MMS[c]
501	37	11	117	71	5	22	0	53	110
701	92	37	78	87	91	69	82	57	90
801	37	44	24	41	54	53	35	37	106
601	40	31	116	139	31				
602	14	21	43	106	8				
604	9	4	7	108	3				
611	78	14	106	134	31				
612	28	7	14	100	8				
614	9	5	9	72	9				
631	94	76	138	389	131				
632	36	14	70	97	66				
634	15	16	30	122	11				

(a) As-deposited metal specimen.
(b) Mixed weld metal specimen.
(c) Mixed weld metal specimen which was reheated to 850°C.

the lowest toughness in the multilayer weld metal, *i.e.*, the weakest region in fracturing is not necessarily located in the as-deposited zone.

Observation of Impact Fracture Surface of the Weld Metal

There is a linear relationship between the distance of cleavage crack origin to the root of notch L_{tc} and absorbed energy E_t as shown in Fig. 7. For most of the specimens, it was observed that the cleavage cracks were initiated from inclusion particles containing Fe, Al, Ti and Mn, and they propagated toward two directions. Figure 8 shows a region around the cleavage origin in a fracture surface. The crack initiation region was a cleavage facet 40–50 μm in size, and the crack origin was an inclusion about 2 μm in size.

Metallographic Examination of the Microstructure in the Crack Initiation Region

By detailed observations of the microstructures of the crack initiation regions on the section shown in Fig. 3A, it is found that for all cases the cleavage cracks were initiated at the regions of the reheated zones in weldments where they were characterized by a group of the most coarse ferrite grains, as shown in Fig. 9B and Table 5. Figure 9A, a photograph of both the fracture surface and the metallographic surface, shows that a cleavage facet is closely related to a ferrite grain. A definite relationship between the size of the ferrite grain in the region of crack initiation and the impact absorbed energy was found as shown in Fig. 10. This was consistent with the results obtained by Ref. 13.

The Remaining Cracks in the Fractured Specimens

Figure 11 shows a typical blunted crack remained in the fractured specimens, as revealed in the metallographic surface shown in Fig. 3B. Some cracks propagated across one ferrite grain, and some of them could cover several ferrite grains. It was found that the length of the maximum remaining crack was inversely related to the impact absorbed energy, as shown in Fig. 12.

Metallographic Observation of the Simulated Microstructure

Figure 13A–D shows the microstructures of the C-Mn weld metals simulated with various peak temperatures and thermal cycles produced during welding with 1 kJ/mm heat input. Figure 13E shows the simulated microstructures of the weld metal produced with 4 kJ/mm heat input, while Fig. 13F shows that of Ti-B weld metal. By observation of all the simulated specimens, it was found that the grain size increased with increasing peak temperature. There was not improvement with

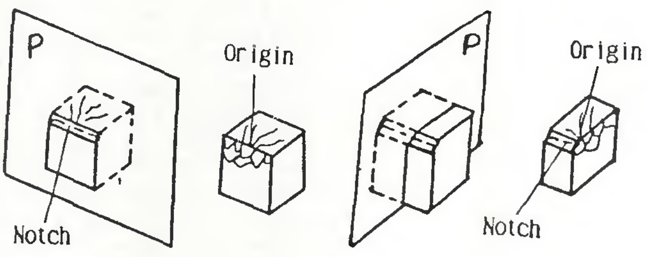

Fig. 3—Fracture-metallography specimens. A— Observing the microstructures in the crack origin zone; B—observing the remaining crack.

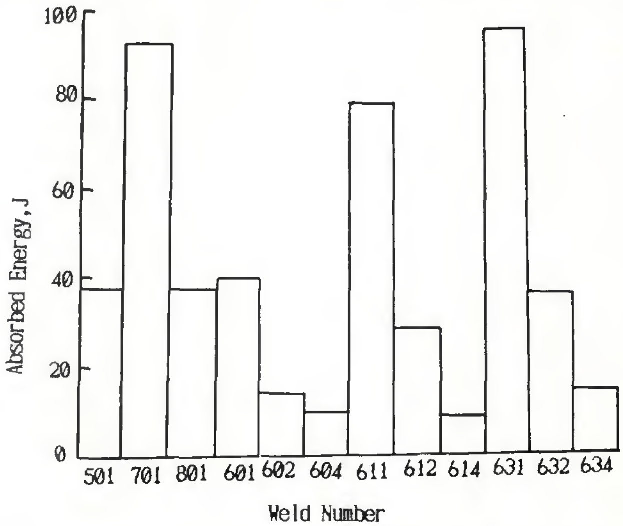

Fig. 4—Absorbed energy of the impacted multilayer weld at −60°C.

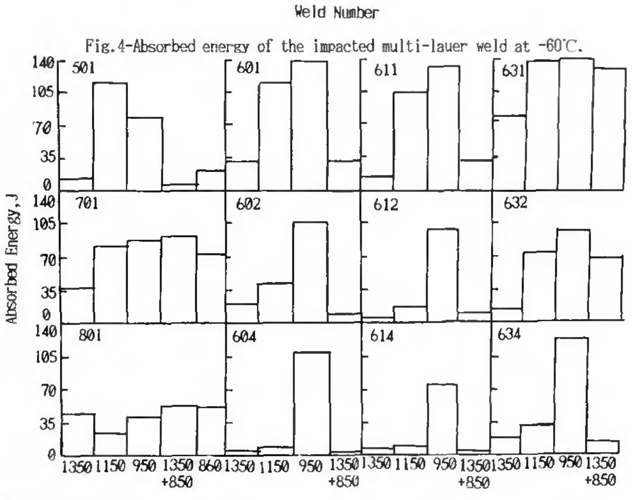

Fig. 5 — Absorbed energy of the simulated specimens tested at −60°C.

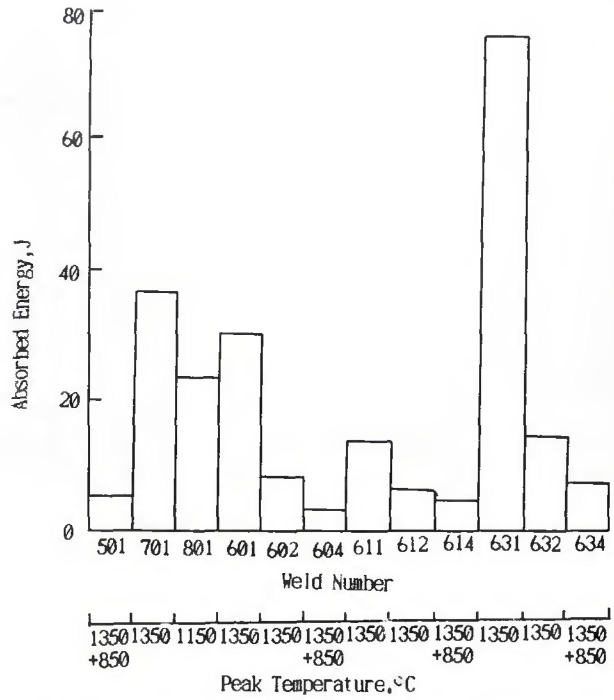

Fig. 6 — The lowest absorbed energy of the simulated specimens.

the double cycle treatment of 850°C. In fact, the short time 850°C treatment made the ferrite grain coarser because only the phase transformation in the subcritical zone occurred. By increasing the heat input of the welding process, the grain size of the double-cycle simulated zone increased greatly. Alloyed with Ti and B, the grain size of that zone was remarkably controlled.

Discussion

The critical length (the length of critical events) that controls impact toughness of the multilayer weld at −60°C was the size of the ferrite grain in the crack initiation region, that is, in the weakest region of fracturing.

Reference 13 revealed that the critical event of unstable cleavage propagation in notched specimens was the extending of the grain size crack through the grain boundary. In this work, it is identified further that, although most cleavage cracks initiated at the inclusion particles as revealed by EDX composition analysis in Fig. 8, the controlling event of cleavage catastrophe was the grain size crack propagation. This viewpoint was supported by the observations noted below.

1) The maximum remaining cracks were of the size of one or several ferrite grain sizes shown in Fig. 11, and the length of the maximum remaining crack was definitely related to the impact absorbed energy, as shown in Fig. 12. It implied that the extending of the crack to failure was controlled by the critical length of the crack produced in the ferrite grain.

2) Figure 8 shows a flat cleavage facet about 40–50 μm around an inclusion initi-

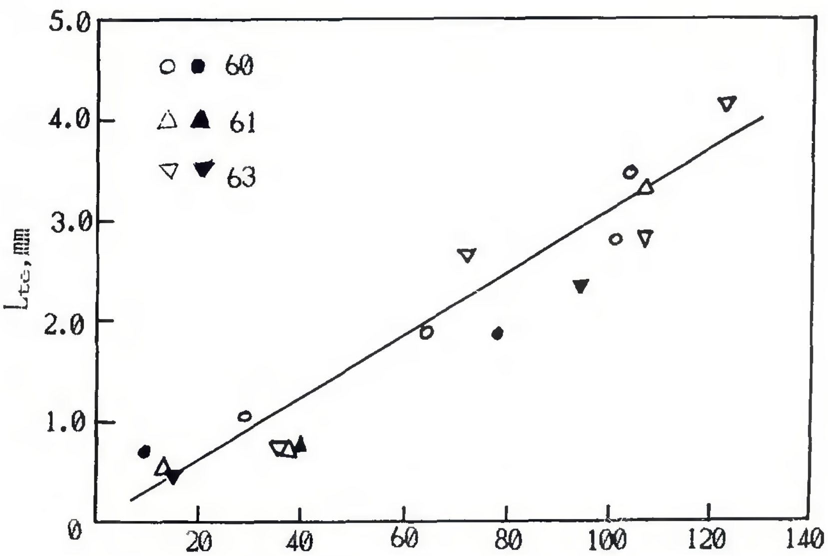

Fig. 7 — The relationship between the distance of cleavage crack origin to the root of the notch L_{tc} and the absorbed energy E_t.

Table 5 — Microstructures in the Zones Initiating Crack (%)

No.	Coarse Ferrite	Acicular Ferrite	Pearlite
501	63.9	36.1	0
701	46.8	53.2	0
801	30.6	69.4	0
601	53.1	42.5	4.4
604	61.9	28.3	9.8
611	48.0	52.0	0
614	84.3	0	12.7
631	44.1	55.9	0
634	90.6	0	9.4

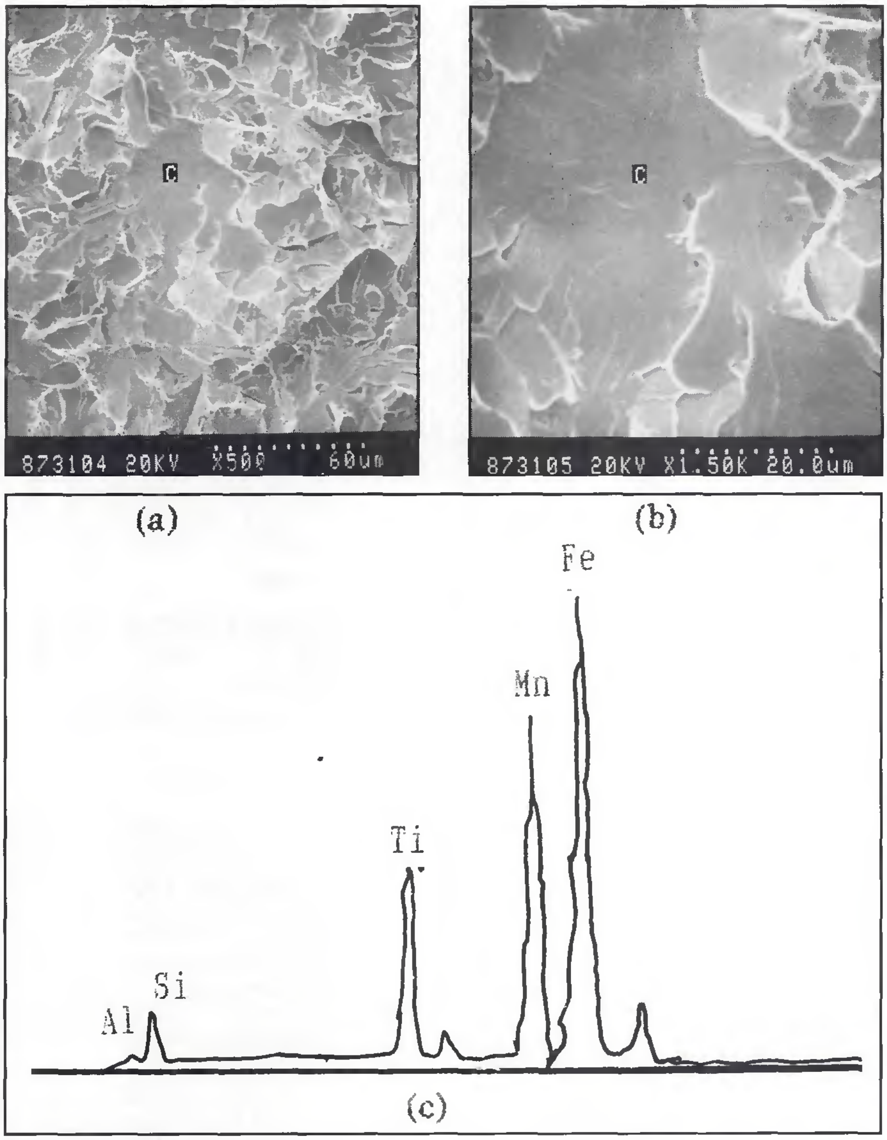

Fig. 8 — Fracture surface and microcrack origin zone of the impacted weld. A — Fracture surface, 500X; B — origin, 1500X; C — EDX analysis of C point in B.

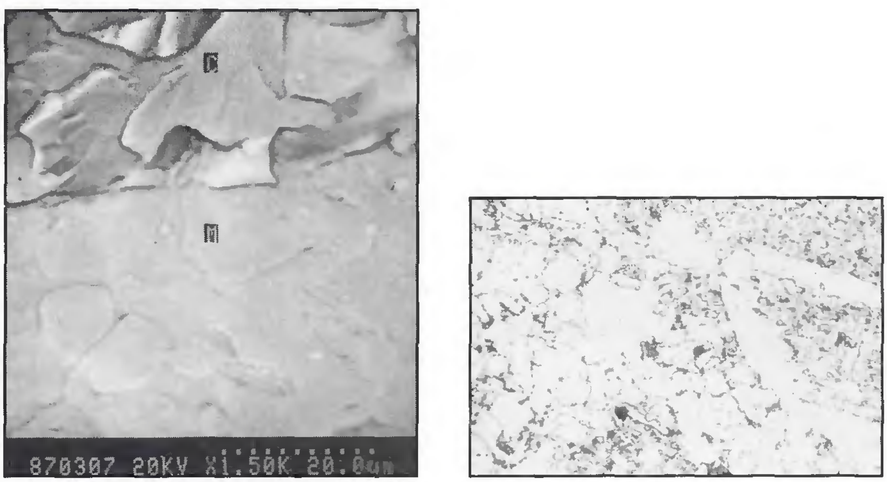

Fig. 9 — The coarse ferrite grain in the crack origin zone. A — SEM image, 1500X; B — optical image, 400X.

ating cleavage crack on the fracture surface, whose size was consistent with that of the remaining crack observed.

3) The crack initiation site was always located in the region characterized by the course grains, as shown in Fig. 9, and the sizes of the coarse grains in these regions were consistent with that of the remaining cracks.

4) There was an apparent relationship between the impact absorbed energy and the diameter of the ferrite grain in the region of crack initiation site as shown in Fig. 10. The impact absorbed energy increased as the size of the ferrite grain decreased. Specifically, when the latter was smaller than 30–40 μm, the former increased rapidly, which identified that the critical length of cleavage catastrophe for Charpy V-notch test at −60°C is around 30–40 μm.

5) The variation of the microstructures shown in Fig. 13 and the toughness shown in Table 4 of the specimens with various alloying elements, heat input and simulated thermal cycles were consistent with the effect of ferrite grain size on the toughness. The larger the grain size produced by the corresponding welding process, the lower the toughness of specimens.

Conclusively, the critical event of impact fracture was the propagation of cracks that initiated from inclusion particles and extended to one or a few ferrite grains in size. The ferrite grain located in the crack initiation region, that is, in the weakest region of fracturing, controlled the extension of the critical cracks and the failure of the whole multilayer welds. This mechanism is different from that investigated by Knott and coworkers (Refs. 10–12), where he considered that cleavage fracture in welds often originated from cracking of oxide inclusions, in particular those situated in the coarse-grained ferrite, and that the size distribution of these inclusions had a significant effect on the fracture toughness.

The region of crack initiation in a fractured multilayer weld is just the lowest toughness zone in the reheated weld.

From Table 4, it can be seen that among all of the specimens, including multilayer welds AMS and MMS, the specimen simulated at a peak temperature of 1350°C or 1350°C +850°C had the lowest toughness. Figure 14 shows the microstructures of the real region of the crack initiation of the multilayer welds and that of the lowest toughness specimen simulated. Obviously, for the weldment with the same composition, it is similar to each other. It means that during the impact test of the multilayer weldment specimen, the cleavage crack was initiated in the zone that had the coarest ferrite grain and the lowest toughness among various reheated zones. For the multilayer welds, specially those that contained higher Mn content, the weakest region is in the reheated zone rather than the deposited metal. As shown

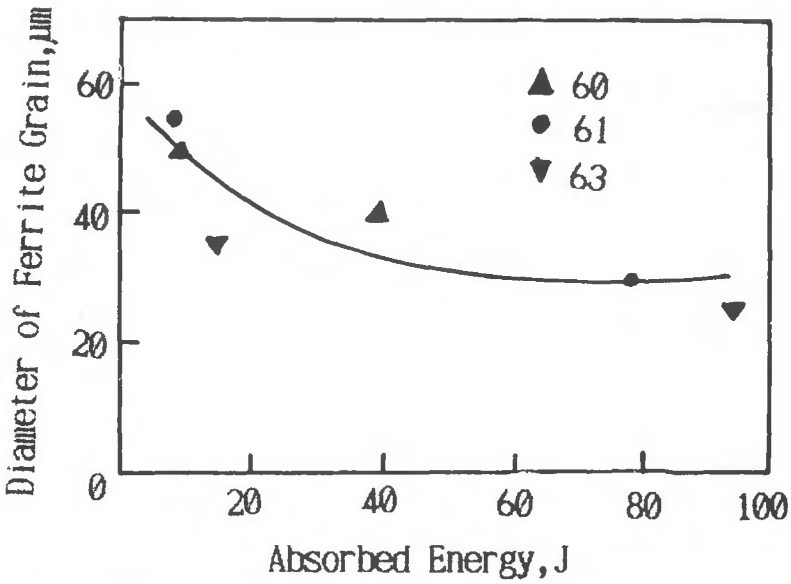

Fig. 10—The relationship between the ferrite grain size and the absorbed energy.

Fig. 11—The remaining crack in the impacted weld, 2000X.

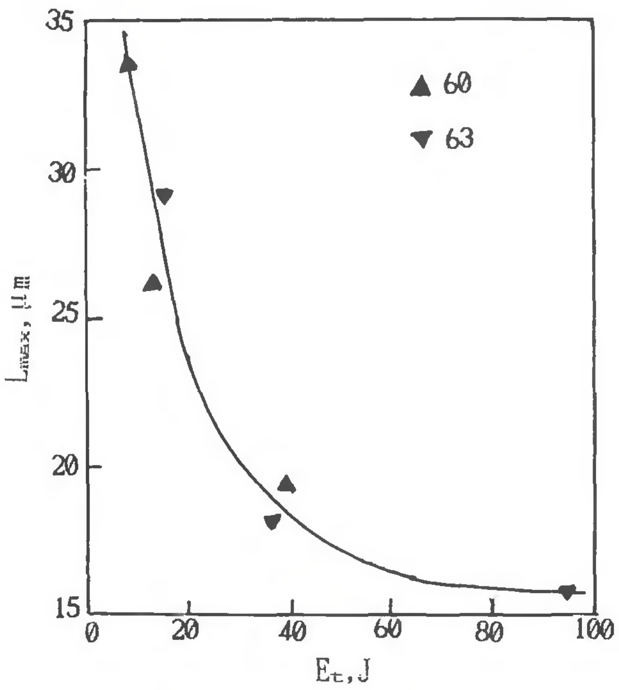

Fig. 12—The relationship between the length of the remaining crack L_{max} and the absorbed energy E_t.

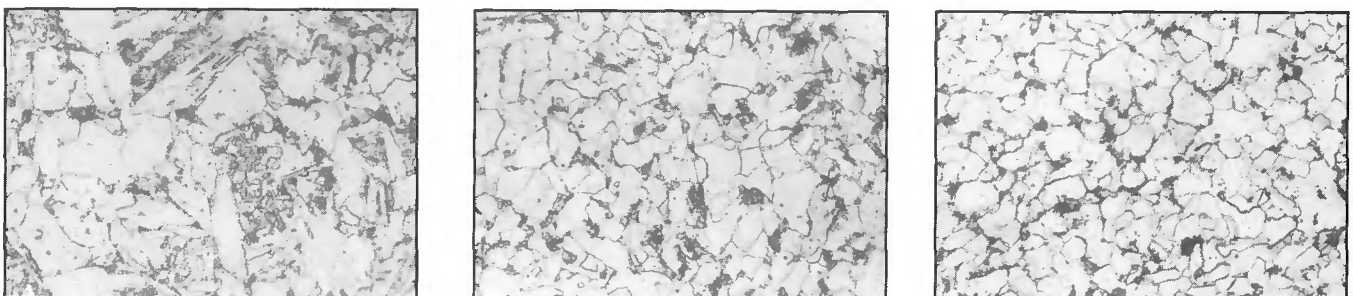

Fig. 13—Microstructures simulated with the different peak temperatures for the different welds. A—601, 1350°C; B—601, 1150°C; C—601, 950°C;

in Fig. 6, the reheated peak temperatures that the weakest region experienced were 1350°C +850°C. For No. 801 weld specimen, which contained the highest Mn in this study, the lowest toughness zone was the zone reheated to 1150°C peak temperature, where a black-strip microstructure was found in this zone.

The toughness of the multilayer weldment depends on that of the lowest toughness zone in the reheated weld.

As shown in Table 6, the trend in variation of impact toughness of the multilayer weldment was followed by the variation of the lowest toughness of various simulated specimens, which just presented the lowest toughness zones of the real reheated welds. The microstructures of the lowest toughness specimens of the simulated weld were uniform, but that of the weakest zone in the practical weld specimens only occurred in a narrow region, and they were surrounded by regions with higher toughnesses. Although the crack initiated in the weakest region and had a permanent effect on the toughness value, it propagated through the region of higher toughness, so that the impact toughness of the weld was higher than that of the lowest toughness zone. However, it can be seen from Table 6 and

Table 6 — The Impact Toughness of the Multilayer Welds, As-Deposited Metals and the Lowest Toughness Zone of the Simulated Welds (J)

No.	Multilayer Weld	The Lowest Toughness of Various Simulated Specimen	As-Deposited Metal
501	37.0	5.3	10.0
701	92.0	37.0	82.7
801	37.0	23.7	34.1
601	39.7	30.7	
602	13.8	7.9	
604	8.8	3.2	
611	78.1	14.0	
612	28.3	6.7	
614	8.6	4.6	
631	94.4	75.9	
632	36.3	14.4	
634	14.8	10.8	

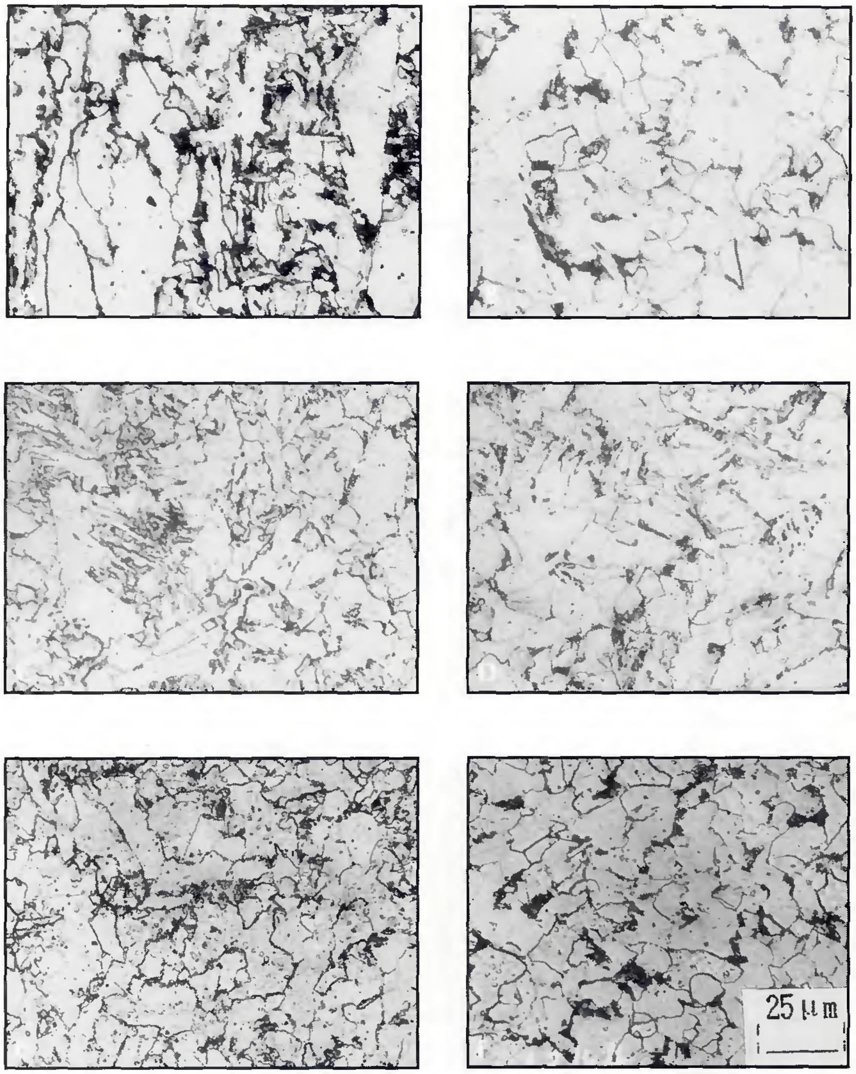

Fig. 14 — Comparison between the microstructure of the specimen having the lowest toughness in the simulated welds with the same composition and that of the crack initiation zone of the impacted weld. A—604; B—604, simulated at 1350°C +850°C; C—611; D—611, simulated at 1350°C; E—634; F—634, simulated at 1350°C + 850°C. 400X

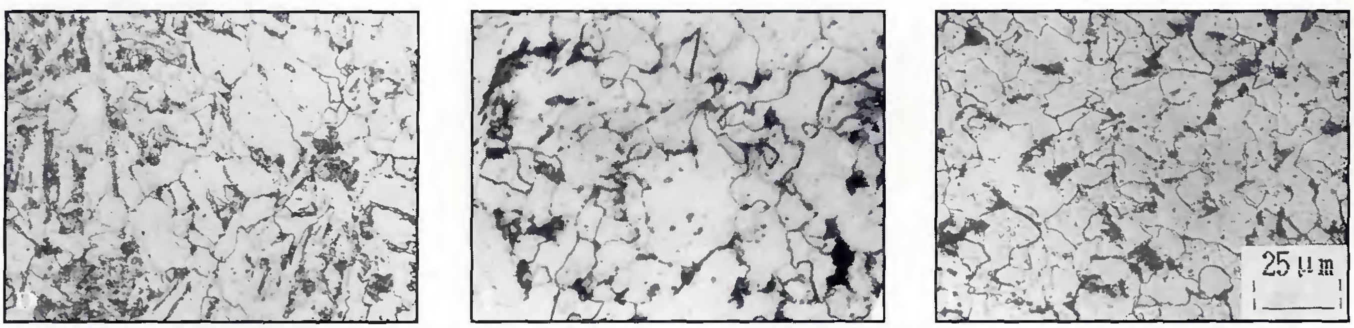

Fig. 13 — continued —. D—601, 1350°C +850°C; E—604, 1350°C +850°C; F—634, 1350°C +850°C 400X.

Fig. 5 that the impact toughness of the multilayer weld at 60°C is closer to that of the weakest region than to that of the other reheated zones.

The reason that Ti, B and Mn increase the toughness of the multilayer weld is their combined effect on refining the ferrite grain in the weakest region.

With increasing heat input, the impact toughness in the multilayer weld decreased because of the dropping of the toughness of the weakest region as shown in Table 6. As heat input increased, the weld experienced more retaining time at high temperature; therefore, in the weakest region, acicular ferrite decreased and coarse ferrite increased and became larger in size, as compared in Fig. 13D and E. The change of the microstructure resulted in a decrease in toughness of the weakest region. The toughness of the whole multilayer weld decreased as well. The factors that improve the toughness of the multilayer weldment are those that decrease the grain size and increase the toughness of the weakest zone of the reheated welds. However, irrespective of how high or low the heat input, the impact toughness of sample No. 63 containing 1.36 wt-% Mn and 240 ppm Ti and 42 ppm B was higher than that of the other two kinds of welds at −60°C. This result is similar with that studied by Oh, *et al.* (Ref. 7).

Conclusively, the method for improving the toughness of the multilayer weld was to decrease the size of the ferrite grain in the weakest region.

Conclusion

1) The critical event controlling the cleavage catastrophe in the impact tested specimen is the propagation of grain size crack through the grain boundary. For the multilayer weld containing 0.68–1.36 wt-% Mn, the weakest region of the weld impact-fractured at −60°C is the coarse ferrite zone reheated with peak temperature of 1350°C or 1350°C +850°C. The exception was the specimen containing 1.98 wt-% Mn. Its peak temperature was 1150°C.

2) The toughness of the multilayer weld is mainly determined by that of the weakest region.

3) The reason that increased heat input decreased the touchness of the weld is because the grain size of the weakest zone increased.

4) Ti, B and Mn combine to increase acicular ferrite and uniform pre-eutectoid ferrite in the coarse-grained zone, decreasing the grain size and increasing the toughness of the weakest zone. This has the effect of increasing the toughness for the whole weldment.

References

1. Stout, R. D., MchLaughin, P. E., and Strunk, S. S. 1969. Heat treatment effects of multipass welds. *Welding Journal* 48(4):115-s to 160-s.

2. Evans, G. M. 1982. Effect of heat input on the microstructure and properties of C-Mn all-weld-metal deposits. *Welding Journal* 61(4): 125-s to 132-s.

3. Evans, G. M. 1980. The effect of manganese on the microstructure and properties of all weld metal deposits. *Welding Journal* 59(3): 67-s to 75-s.

4. Tsuboi, J., and Terashima, H. 1980. Reviews of strength and toughness of Ti-B microalloying deposits. IIW-doc. IX-28-80.

5. Mori, N., Homma, H., Wakabayaski, M., and Ohkita, S. 1982. Characteristics of mechanical properties of Ti-B bearing weld metals. IIW-doc-II-980-82.

6. Kohno, R., Takami, T., Mori, W., and Nagano, K. 1982. New flux of improved well metal toughness for HSLA steels. *Welding Journal* 61(12):373-s to 380-s.

7. Oh, D. W., Oison, D. L., and Frost, R. H. 1990. The influence of boron and titanium on low-carbon steel weld metal. *Welding Journal* 69(4):151-s to 158-s.

8. Koshio, T., Ootawa, M., Tanigaki, R., Takino, T., Horii, Y., Tsunetomi, E., and Imai, K. 1981. Development of the high-COD titanium and boron bearing covered electrode. IIW-doc. II-955-81.

9. Lathabai, S., and Stout, R. D. 1985. Shielding gas and heat input effects on flux cored weld metal properties. *Welding Journal* 64(11): 303-s to 313-s.

10. Tweed, J. H., and Knott, J. F. 1987. The effect of preheat temperature on the microstructure and toughness of a C-Mn weld metal. *Met. Constr.* 19(3):153R–158R.

11. Mcrobie, D. E, and Knott, J. F. 1985. Effects of strain aging on fracture toughness of C-Mn weld metal. *Mater. Sci. and Tech.* (5):357–365.

12. Tweed, J. H., and Knott, J. F. 1987. Micromechanisms of failure in C-Mn weld metals. *Acta Met.* 35(7):1401–1414.

13. Chen, J. H., and Yan, C. 1988. Fracture behavior of C-Mn steel multipass MMA weld metals at −60°C in Charpy V testing. *Mater. Sci. and Tech.* 4(8):732–739.

14. Evans, G. M. 1985. The effects of heat treatment on the microstructure and properties of C-Mn all weld metal deposits. *Met. Constr.* 17(10):676R–682R.